


Research Article

Segmentation for Human Motion Injury Ultrasound Medical Images Using Deep Feature Fusion

Jingmeng Sun and Yifei Liu 

Physical Education Department, Harbin Engineering University, Harbin 150001, China

Correspondence should be addressed to Yifei Liu; liuyifei@hrbeu.edu.cn

Received 26 May 2022; Revised 14 July 2022; Accepted 29 July 2022; Published 29 August 2022

Academic Editor: Xiaofeng Li

Copyright © 2022 Jingmeng Sun and Yifei Liu. This is an open access article distributed under the Creative Commons Attribution License, which permits unrestricted use, distribution, and reproduction in any medium, provided the original work is properly cited.

Image processing technology assists physicians in the analysis of athletes' human motion injuries, not only to improve the accuracy of athletes' injury detection but also to improve the localization and recognition of injury locations. It is important to accurately segment human motion injury ultrasound medical images. To address many problems such as poor effect of traditional ultrasonic medical image segmentation algorithm for a sports injury. Therefore, we propose a segmentation algorithm for human motion injury ultrasound medical images using deep feature fusion. First, the accurate estimated value of human posture is extracted and combined with image texture features and image gray value as the target feature value of the ultrasonic medical image of human motion injury. Second, the image features are deeply fused by an adaptive fusion algorithm to enhance the image resolution. Finally, the best segmentation value of the image is obtained by the trained support vector machine to realize the accurate segmentation of human motion injury ultrasonic medical image. The results show that the average accuracy of the posture accurate estimation of the proposed algorithm is 95.97%; the segmentation time of the human motion injury ultrasound medical image of the proposed algorithm is below 150 ms; and the convergence of the algorithm is completed when the number of iterations is 3. The maximum segmentation error rate is 2.68%. The image segmentation effect is consistent with the ideal target segmentation effect. The proposed algorithm has important application value in the field of ultrasonic medical diagnosis of sports injury.

1. Introduction

Human motion analysis is to use relevant methods to track and capture human motion parameters, so as to reconstruct human structure and posture and achieve the goal of estimating and identifying human structure and posture [1]. With the continuous progress of image processing technology [2], using image processing technology to assist doctors in human motion injury analysis of athletes is one of the focuses of scholars at home and abroad in recent years. Using image processing technology to process the ultrasonic medical image of the injured part of human motion athletes not only can improve the injury detection of athletes but also can improve the ability to locate and identify the injured position. Therefore, the ultrasonic medical image segmentation algorithm for human motion injury has very important research significance.

Yan et al. [3] proposed an image segmentation algorithm based on a level set. First, the algorithm obtains the value of the image symbol function through the calculation of the objective function, determines the relevant constraints, and establishes the image segmentation model. Finally, the image contour segmentation is completed based on the established model and the set relevant initial curve, but the algorithm is too complex and has the practical problem of long segmentation time. Liu et al. [4] proposed the ore image segmentation algorithm based on U-Net and Res-Unet convolution networks. First, the algorithm implements gray value and median filtering to complete image denoising and uses the histogram equalization method to extract the image target position. And then, based on U-net and Res-U-net convolution network, the image contour segmentation model is constructed; finally, the image segmentation is realized through the image segmentation model. However,

in practical application, it is found that the convergence speed of this algorithm is slow and the practical application effect is poor. Sediqi and Lee [5] proposed an image semantic segmentation algorithm based on new sampling and context convolution. The algorithm preserves the spatial information of the image based on the guidance filter; then, the local context convolution method is used to cover the target in the image, and the accurate boundary description is carried out; and finally, the accurate segmentation of the image is realized by depicting the results. However, this algorithm has a high segmentation error rate and poor practical application effect. Lin and Li [6] proposed a parallel region segmentation algorithm for high-resolution remote sensing images based on a minimum spanning tree. The algorithm divides the image into several pixel blocks according to the conventional mosaic algorithm. Based on the multicore parallel method, the image segmentation rules are obtained, and the minimum spanning tree model is established. Finally, the model is solved by the parallel merging method to realize image segmentation. However, the segmentation time of this method is poor, which is quite different from the ideal application effect. Xue et al. [7] proposed an image segmentation algorithm based on improved FCN-8s. First, the algorithm establishes the image data set, extracts the image features according to the multiscale feature extraction method, and then establishes the convolution network model of the image. Finally, the image segmentation is realized through the output of the model. However, this method has a slow convergence speed and is difficult to achieve the expected goal.

The above image segmentation algorithm fails to fuse the image pixel values. Therefore, the above algorithm has the problems of long segmentation time, slow convergence speed, high segmentation error rate, and poor segmentation effect. In order to address these problems, this paper proposes a human motion injury ultrasonic medical image segmentation algorithm based on deep feature fusion. The contributions of this paper are as follows: (1) according to the accurate estimation of human posture, image texture features, and image gray value, the image target feature value is obtained, which improves the accuracy of feature extraction. (2) This study uses the advantages of fast speed and high precision of support vector machine to realize accurate image segmentation and puts forward the quality and efficiency of image segmentation. (3) Multiple data sets are selected for testing to prove that this algorithm has certain advantages in cutting time, convergence speed, segmentation error rate, segmentation effect, and so on.

2. Methodology

Before the image segmentation of human motion injury ultrasonic medical image [8, 9], it is necessary to give priority to estimating the athlete's motion posture and take it as the feature of the medical ultrasonic image to assist in the segmentation of the medical ultrasonic image.

2.1. Analysis of Human Motion Trajectory of Athletes. The high-definition camera is used to capture the athlete's motion process, obtain the athlete's motion video image, and complete the motion trajectory analysis of the athlete's human parts on this basis [10, 11].

2.1.1. Trajectory Analysis of Human Single Part. Set the single part appearance test item of human as $\Omega_a(b)$, and $\Phi_a(b_t, b_{t+1})$ is similarity measure, as to complete the motion trajectory expression of a single part of the human. The process is as follows:

$$\left\{ \begin{array}{l} \Omega_a(b) = \sum_{i=1}^C \left(\Omega(b_i) + \sum_{n=1}^{D-1} \beta_n \|b_i \neq b_i^n\| \right), \\ \Phi_a(b_t, b_{t+1}) = \\ \exp \left(-\frac{\alpha^2 (T(b_t), T(b_t + b_{t+1})) \|\hat{b}_t - b_{t+1}\|_2^2}{\theta^2} \right), \end{array} \right. \quad (1)$$

where the image frame of the human single part motion image is described by t and $(t + 1)$. β_n is Lagrange multiplier; D denotes the total number of multipliers; and C is the single part appearance feature set. The appearance of athletes' human parts is described by $\Omega(b_i)$, and b is the position of athletes' human parts in the image frame. α^2 is chi-square operator. $T(b)$ is local HOG feature coefficient [12]; θ is a relevant parameter; and \hat{b}_t is the predicted location of the $(t + 1)$ image frame through streamer prediction.

According to the above calculation results, set the athlete's single part status configuration parameter as χ_i^e to obtain the athlete's single part trajectory. The process is as follows:

$$E_e(\chi^e) = \sum_{i=1}^L \Omega_a(\chi_i^e) + \sum_{i=1}^{L-1} \Phi_a(\chi_i^e, \chi_{i+1}^e), \quad (2)$$

where $E_e(\chi^e)$ is the athlete's single part trajectory, χ^e is video sequence, L denotes the number of video frames, the optimization function of athlete's single part trajectory [13] is described by E_e , and i is the constant.

2.1.2. Analysis of Athlete's Symmetrical Part Trajectory. Based on the analysis of the trajectory of single parts of the human, the trajectory of symmetrical parts of athletes is analyzed, so as to realize the analysis of the trajectory of athletes' human motion. Since the positions of symmetrical parts are left and right symmetrical, it is necessary to obtain their positions through the position coordinates of x, y . Set the athlete's compound coordinate position as $f = (x, y)$ to obtain the appearance feature of the athlete's symmetrical part. The specific results are as follows:

$$\Omega_\varepsilon(f) = \frac{(\Phi_a(f, x) + \Phi_a(f, y)) \times (\wedge(f, x)^T \cdot \wedge(f, x))}{(1 + g^{-\wedge f, x-f, y|/K})}, \quad (3)$$

where the expression of the athlete's symmetrical part is marked in the form of $\Phi_a(f, x)$ and $\Phi_a(f, y)$. g is the penalty function of the symmetrical part; K denotes the penalty coefficient; and \wedge stands for the color histogram of the human motion image.

Finally, based on the above calculation results, the motion track of athletes' symmetrical parts is obtained, and the process is as follows:

$$E_\varepsilon(\chi^\varepsilon) = \sum_{i=1}^L \Omega_\varepsilon(\chi_i^\varepsilon) + \sum_{i=1}^{L-1} \Phi_\varepsilon(\chi_i^\varepsilon, \chi_{i+1}^\varepsilon), \quad (4)$$

where χ^ε is video sequence, χ_i^ε represents status configuration set of symmetrical parts of athletes, and E_ε is the target optimization function.

2.2. Establishment of an Accurate Estimation Model of Athletes' Motion Posture. According to the analysis results of athletes' human motion trajectory, an accurate estimation model of athletes' motion posture is constructed to realize the accurate estimation of athletes' motion posture. The athletes' motion posture can be expressed by three-dimensional coordinates with p nodes. To reduce the fuzziness of athletes' motion posture estimation results, it is assumed that the athletes' motion posture to be estimated can be linearly represented by a set of predefined basic postures. The athlete's motion posture model in the video can be expressed in the following equation:

$$S_t = \sum_{i=1}^k c_{it} B_i, \quad (5)$$

where t represents the value of frame t of the athlete's motion video, B_i represents the basic posture of athletes, k represents the number of atoms of the basic posture B_i , and c_{it} is the coefficient of base posture B_i .

The two-dimensional posture of each frame of the athlete's motion video can be obtained by translating and rotating the corresponding three-dimensional posture. Therefore, the projection relationship between the athlete's two-dimensional posture and its corresponding athlete's three-dimensional posture can be expressed by the following equation:

$$W_t = (R_t S_t + T_t 1^T), \quad (6)$$

where R_t and T_t represent the camera translation vector and rotation matrix, respectively, and T represents matrix transpose.

Supposed that W , R , and T represent the set of W_t , R_t , and T_t of all frames, respectively.

$\theta = \{C, R, T\}$ is the overall parameter of the athlete's three-dimensional posture coordinates. $L(\theta; W)$ is the loss function, expressed as follows:

$$L(\theta; W) = \frac{\nu}{2} \sum_{i=1}^n \left\| W_t - R_t \sum_{i=1}^k c_{it} B_i - T_t 1^T \right\|_F^2, \quad (7)$$

where $\| * \|_F$ is the F norm of the representative matrix and ν represents the projection variance of athletes' three- to two-dimensional posture.

According to the above results, the athlete's motion posture model is optimized, and the optimization results are

$$S_t = \frac{\nu}{2} \sum_{i=1}^k c_{it} R_{it} B_i. \quad (8)$$

Set the fixed components of the model as $\eta = 26$ and local mixing type as $\mu = 4$, and A is the top of the model. δ is edge set of connected parts of human; $B = \{b_i\}_{i=1}^K$ denotes location collection of human parts; and χ_i is human part status configuration, so as to establish the accurate estimation model of athlete's posture [14]. The process is as follows:

$$M(\chi) = \frac{\sum_{\chi_i \in \chi} \Omega(\chi_i) + \sum_{\chi_i, \chi_j \in \chi} \gamma(\chi_i, \chi_j)}{A} \delta, \quad (9)$$

where $M(\chi)$ is the established accurate athlete's posture prediction model, $\gamma(\chi_i, \chi_j)$ is the athlete injury scoring item, $\Omega(\chi_i)$ stands for appearance features of human parts, and the part compatibility of the top of a human $A = (\nu_i, \nu_j)$ is marked in the form of b_i and b_j .

2.3. Accurate Estimation Process of Athletes' Posture. The specific accurate estimation process of an athletes' posture is shown in Figure 1.

According to the data in Figure 1, the accurate estimation process of athlete's posture is to capture the athlete's motion process through the high-definition camera, obtain the athlete's motion video image, and complete the image acquisition. On this basis, the human position and the initial position of each part of the human in a single frame image are estimated. According to the relevant estimation results, the relevant constraint relationship of human part posture estimation is established, so as to build the relevant posture estimation model. By obtaining the motion trajectory of human parts, the model is optimized, and the accurate estimated value of athlete posture is output.

2.4. Segmentation Algorithm of Athletes' Injury Ultrasonic Image. Taking the accurate estimated value of athletes' posture obtained above as the target feature of athletes' injury ultrasonic image, SVM [15] is used to segment athletes' injury ultrasonic image.

2.4.1. Image Segmentation Recognition. According to the determined image features and high-resolution CT scanning algorithm, the high-resolution information sampling equation of medical ultrasound image is obtained [16]. The process is as follows:

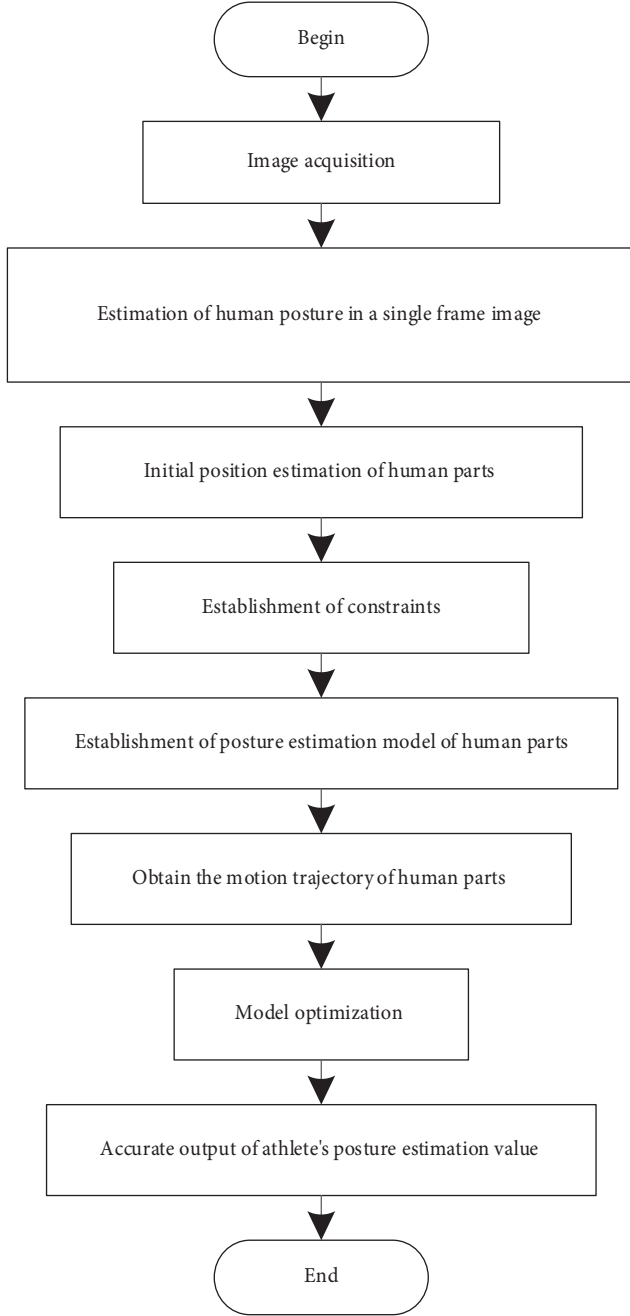


FIGURE 1: Accurate estimation process of athletes' posture.

$$\begin{cases} \dot{m}(r) = -Gm(r) + Hf(n(r - \lambda)), \\ \dot{n}(r) = -On(r) + Pm(r - \varphi), \end{cases} \quad (10)$$

where pixel acquisition point of ultrasonic medical image is marked in the form of G , H , O , and P . $m(r)$ is pixel length of the injured part of the athlete in the image; $n(r)$ is the width; and the domain decomposition value of information feature fusion for human motion injury is marked in the form of λ and φ .

Because the acquired image features are not a kind of athlete's posture estimation value, it is necessary to deeply

fuse the image features. Set the similarity feature of the ultrasonic medical image as $w(m, n)$; $Ncut(m, n)$ is the image gray histogram; and (x, y) denotes the gray pixel set, so as to establish feature decomposition model of ultrasonic image [17]. The process is as follows:

$$F_{fjz}(x, y_m) = \frac{1}{\sqrt{xQ}} \left(\left(\frac{Q}{2} + \frac{xQ}{2} \right) - y_m \right), \quad (11)$$

where $z(x, y_m)$ is image texture output, Q stands for feature decomposition coefficient, $F_{fjz}(x, y_m)$ is the established feature decomposition model, and m is the constant.

According to the adaptive fusion algorithm, the pixel value of medical ultrasound image is fused, and the deep feature fusion output of the medical ultrasound image is completed. The calculation equation is as follows:

$$R(a) = \left[J(a) - \frac{S_{zj}}{\max(t(a), t_0)} \right] + S_{zj}, \quad (12)$$

where $R(a)$ is feature fusion output value of medical ultrasound image, S_{zj} is image pixel subset, $J(a)$ represents the gray image [18, 19], t_0 is the image initial structure similarity, and $(t(a), t_0)$ denotes the similarity degree.

2.4.2. Proposed Algorithm. The process of ultrasonic medical image segmentation algorithm for human motion injury is as follows:

Input: ultrasonic medical image of human motion injury

Output: image segmentation results

- (1) Based on the deep feature fusion results of human motion injury ultrasonic medical image, the corresponding constraints are formulated to reduce the segmentation surface error of ultrasonic image. First, the fusion evaluation result of the human motion injury image is set as v , and the image matching evaluation function is marked as $v(g_j)$. Based on this, the distance between the pixel and the cluster center in the human motion injury image is calculated, and the pixel gray output of the visual graphics of the human motion injury image is obtained, which is used as the pathological characteristic value of the ultrasonic image. The calculation equation is as follows:

$$\vartheta = \arccos \left\{ \left[\frac{\overrightarrow{Z_i W_k} \times \overrightarrow{Z_i Z_j}}{\|\overrightarrow{Z_i W_k}\| \cdot \|\overrightarrow{Z_i Z_j}\|} \right]_{\max} \right\}, \quad (13)$$

where ϑ is the pixel gray output value is marked. W_i is the gradient direction position value of the image, and $\overrightarrow{Z_i Z_j}$ denotes the image rendering vector.

- (2) According to the above calculation results, the fusion region constraint is carried out on the visual graphics of the ultrasonic image, and the threshold segmentation value of SVM is obtained. The calculation equation is as follows:

$$\xi(m, n) = \frac{1}{T(i)} \exp\left(-\frac{c(m, n)}{\rho^2}\right), \quad (14)$$

where $\xi(m, n)$ is the optimal segmentation threshold, $T(i)$ denotes the best match value of the image template, ρ^2 is a constraint parameter, and $c(m, n)$ stands for the feature point of the pixel. Finally, the feature fusion value is minimized by a priori energy function to obtain the best segmentation output value. The calculation equation is as follows:

$$f(x) = (r_\rho x - r_\rho x_1), \quad (15)$$

where $f(x)$ is the optimal segmentation and output of ultrasonic medical images of human motion injury, r_ρ is statistical features of ultrasonic images, and x is image edge subset.

- (3) According to the optimal segmentation value of SVM, the ultrasonic pathological feature is adaptively segmented, so as to realize the accurate segmentation of human motion injury ultrasonic medical images [20].

The process of ultrasonic medical image segmentation algorithm for sports injury based on deep feature fusion is shown in Figure 2.

3. Experimental Analysis and Results

3.1. Data Set. In this paper, MedPix data set and MURA data set data sets are selected for the experiment. MedPix data set is a free and open online access database, which contains medical images, teaching cases, and clinical topics and integrates image and text metadata, including more than 12,000 patient cases, 9,000 topics, and nearly 59,000 images. Our main target audience includes doctors and nurses, full-time medical personnel, medical students, nursing students, and others who are interested in medical knowledge. The content materials are organized according to the location of the disease (organ system) and pathological category and patient data and through image classification and image title. The collection can be searched by patient symptoms and signs, diagnosis, organ system, image form and image description, keywords, contributing authors, and many other search options. MURA data set is one of the largest public ray image data sets produced by the Stanford machine learning working group. MURA is a data set of musculoskeletal radiographs. It contains a total of 14,863 studies in 12,173 patients and 40,561 multiview ultrasound radiographs, including fingers, elbows, forearms, hands, humerus, shoulders, and wrists.

Integrated the data in the two data sets and input all the experimental sample data into the simulation software. Randomly select 2,000 images in two data sets to test the segmentation error rate. Eighty percent of the data is used for training, and 20% of the data is used for testing. After many tests, the optimal operating parameters of the simulation software are obtained, and relevant experiments are

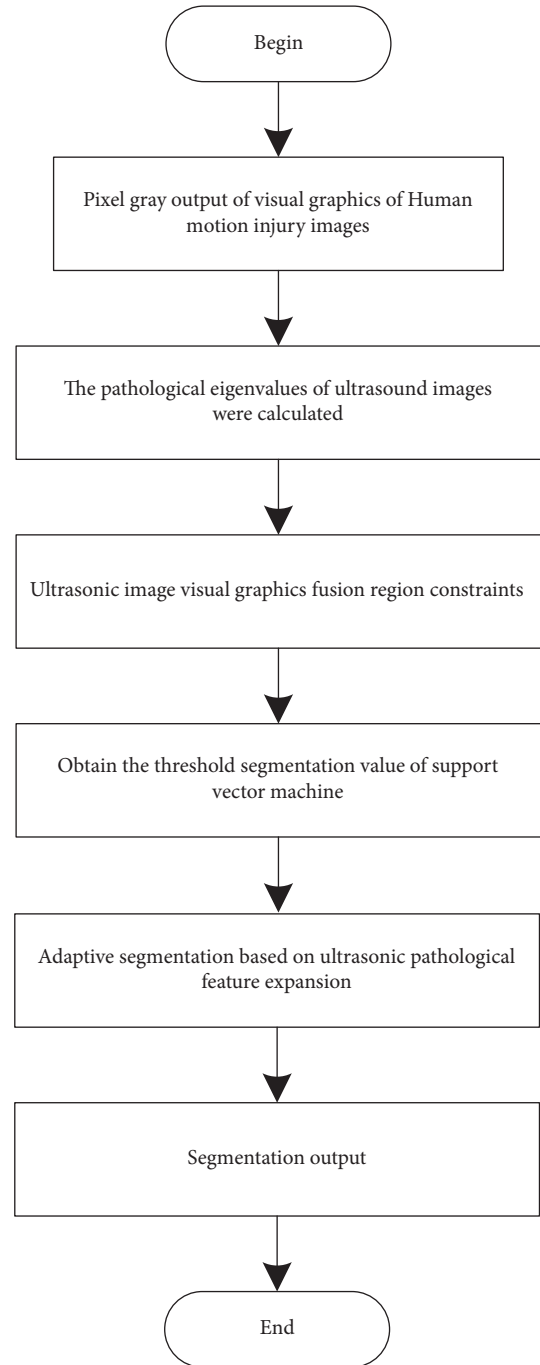


FIGURE 2: The proposed algorithm process.

carried out under these parameters, so as to ensure the authenticity and reliability of the experimental results.

3.2. Experimental Standard. The proposed algorithm of human motion injury based on deep feature fusion, algorithm (algorithm 1) proposed by literature [3], algorithm (algorithm2) proposed by literature [4], algorithm (algorithm 3) proposed by literature [5], algorithm (algorithm 4) proposed by literature [6], and algorithm (algorithm 5) proposed by literature [7], were used for testing. In the process of image segmentation, the segmentation

TABLE 1: Accuracy of athletes' posture accurate estimation.

Number of images/piece	Estimated accuracy (%)					
	Proposed algorithm	Algorithm 1	Algorithm 2	Algorithm 3	Algorithm 4	Algorithm 5
100	95.63	85.63	85.63	85.64	75.41	69.36
200	96.84	87.49	84.75	87.45	86.39	75.64
300	97.56	86.33	90.12	71.36	84.75	75.88
400	96.31	85.94	87.11	74.56	82.31	74.63
500	95.22	82.37	78.63	82.35	74.56	85.12
600	98.17	84.19	85.26	79.63	72.35	87.65
700	96.33	85.67	74.16	78.41	74.18	85.22
800	95.14	85.61	71.33	71.63	84.36	84.79
900	92.37	84.75	79.63	85.36	76.33	86.31
1,000	96.17	83.69	85.23	80.12	84.15	84.54
Average value	95.97	85.16	82.19	79.65	79.48	80.91

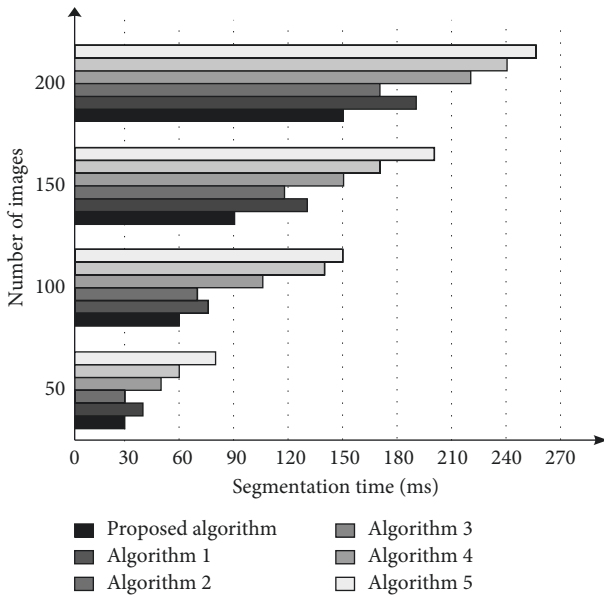


FIGURE 3: Comparison of segmentation time test results of different segmentation algorithms.

performance of segmentation algorithm is the key to reflect the effectiveness of segmentation algorithm. When using the proposed algorithm, algorithms 1–5 to carry out image segmentation, several test indexes such as accuracy, segmentation time, convergence speed, segmentation error, and segmentation effect are selected to test the segmentation performance of the above six image segmentation algorithms.

- (1) Accuracy of athlete's posture estimation: this indicator refers to the probability of accurately estimating an athlete's posture. The calculation equation is as follows:

$$f = \frac{z_i}{z_j} \times 100\%, \quad (16)$$

where z_i refers to the amount of data about the accurately estimate athlete's posture and z_j refers to the total amount of athlete's data sample.

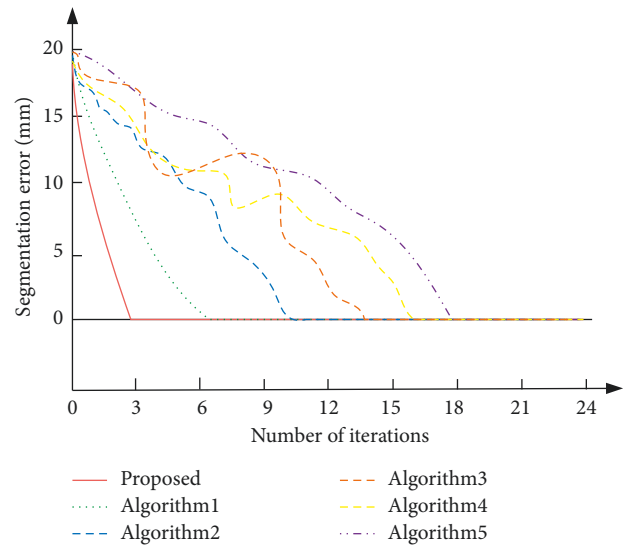


FIGURE 4: Comparison of convergence test results.

- (2) Segmentation time: this indicator is only the sum of the time taken to complete the segmentation steps of ultrasonic medical images of human motion injury. The calculation equation is as follows:

$$t = \sum_{i=1}^n T_i, \quad (17)$$

where T_i represents the time taken for the i -th division step.

- (3) Convergence speed: this indicator refers to the number of iterations when the segmentation error of ultrasonic medical images of human motion injury is the lowest. The less the number of iterations, the faster the convergence speed.
- (4) Segmentation error rate: this index refers to the ratio of the number of correctly segmented images to the total number of experimental samples. The calculation equation is as follows:

$$e = \frac{o}{p} \times 100\%, \quad (18)$$

TABLE 2: Comparison of segmentation error rate test results of different segmentation algorithms.

Number of images/piece	Segmentation error rate test result (%)					
	Proposed algorithm	Algorithm 1	Algorithm 2	Algorithm 3	Algorithm 4	Algorithm 5
100	0	0	0	0.11	0.27	0.42
200	0	0	0.10	0.47	0.61	1.04
300	0	0.22	0.48	1.13	1.55	2.08
400	0.25	0.39	0.99	1.88	2.03	3.43
500	0.47	0.58	1.57	2.59	3.21	4.57
600	0.89	1.05	2.03	3.01	4.08	5.29
700	1.23	1.64	2.84	3.99	5.12	6.43
800	1.79	2.08	3.42	4.58	6.25	7.14
900	2.37	2.51	4.05	5.01	7.39	7.92
1,000	2.68	3.16	4.92	5.76	8.01	8.50

where o refers to the number of correctly segmented images, and p refers to the total amount of experimental samples.

- (5) Segmentation effect test: the closer the segmentation results of different algorithms are to the ideal segmentation results, the better the segmentation effect of human motion injury ultrasonic medical image.

3.3. Results and Discussion. The accuracy of athletes' posture accurate estimation of the proposed algorithm, algorithm 1, algorithm 2, algorithm 3, algorithm 4, and algorithm 5 are compared. The comparison results are shown in Table 1.

According to the data in Table 1, the average accuracy of an athlete's posture estimation of the proposed algorithm is 95.97%. The average accuracy of an athlete's posture estimation of algorithm 1 is 85.16%. The average accuracy of an athlete's posture estimation of algorithm 2 is 82.19%. The average accuracy of an athlete's posture estimation of algorithm 3 is 79.65%. The average accuracy of an athlete's posture estimation of algorithm 4 is 79.48%. The average accuracy of an athlete's posture estimation of algorithm 5 is 80.91%. Compared with the experimental comparison algorithm, the accuracy of an athlete's posture estimation of algorithm in this paper is higher, and the estimation effect is better.

In the process of image segmentation, the segmentation time is the key index to display the segmentation performance of the segmentation algorithm. The above six image segmentation algorithms are used to carry out image segmentation and test the image segmentation time of the six algorithms, as shown in Figure 3.

It is seen in Figure 3 that in the process of image segmentation, the longer the segmentation time, the worse the segmentation performance of the segmentation algorithm, and the shorter the segmentation time, the higher the segmentation performance. By analyzing Figure 3, it can be seen that with the increase in detection times, the segmentation time of the six image segmentation algorithms has increased to varying degrees. The segmentation time of ultrasonic medical image of sports injury in the proposed algorithm is less than 150 ms, which is 45 ms, 19 ms, 71 ms, 90 ms, and 105 ms lower than algorithms 1–5, respectively.

The proposed algorithm has the shortest image segmentation time among the six segmentation algorithms. This is because the proposed algorithm uses an adaptive fusion algorithm to fuse the image pixel values during image segmentation. Therefore, the segmentation time of the proposed algorithm in image segmentation is better than the other five image segmentation algorithms.

When carrying out image segmentation, the convergence speed of the segmentation algorithm is an important process to detect the segmentation performance of the segmentation algorithm. The above six image segmentation algorithms are used to carry out image segmentation, and the segmentation convergence speed of the six algorithms is tested, as shown in Figure 4.

According to Figure 4, in the process of image segmentation, the faster the convergence speed, the better the image segmentation performance, and vice versa. By analyzing the experimental data in Figure 4, it can be seen that the proposed algorithm completes the convergence of the algorithm when the number of iterations is 3, and the number of convergence is 4, 8, 11, 14, and 15 lower than algorithms 1–5, respectively. In general, the convergence speed of other algorithms is lower than that of the proposed algorithm, and the convergence speed of algorithm 4 is the most unstable. It can be proved that the proposed algorithm has a high convergence speed when implementing image segmentation.

In the process of image segmentation, the level of image segmentation error can directly affect the segmentation performance of the segmentation algorithm. When using the proposed algorithm, algorithms 1–5 to perform image segmentation, the segmentation error rates of six image segmentation algorithms are tested. It is shown in Table 2.

The larger the segmentation error, the worse the segmentation performance of the segmentation algorithm, and vice versa. It can be seen from Table 2 that the more images to be segmented, the greater the segmentation error measured by the six algorithms. The maximum segmentation error rate of the proposed algorithm is 2.68%, which is 0.48%, 2.24%, 3.08%, 5.33%, and 5.82% lower than algorithms 1–5, respectively. Overall, the test result of the proposed algorithm is the image segmentation algorithm with the smallest error among the six image segmentation

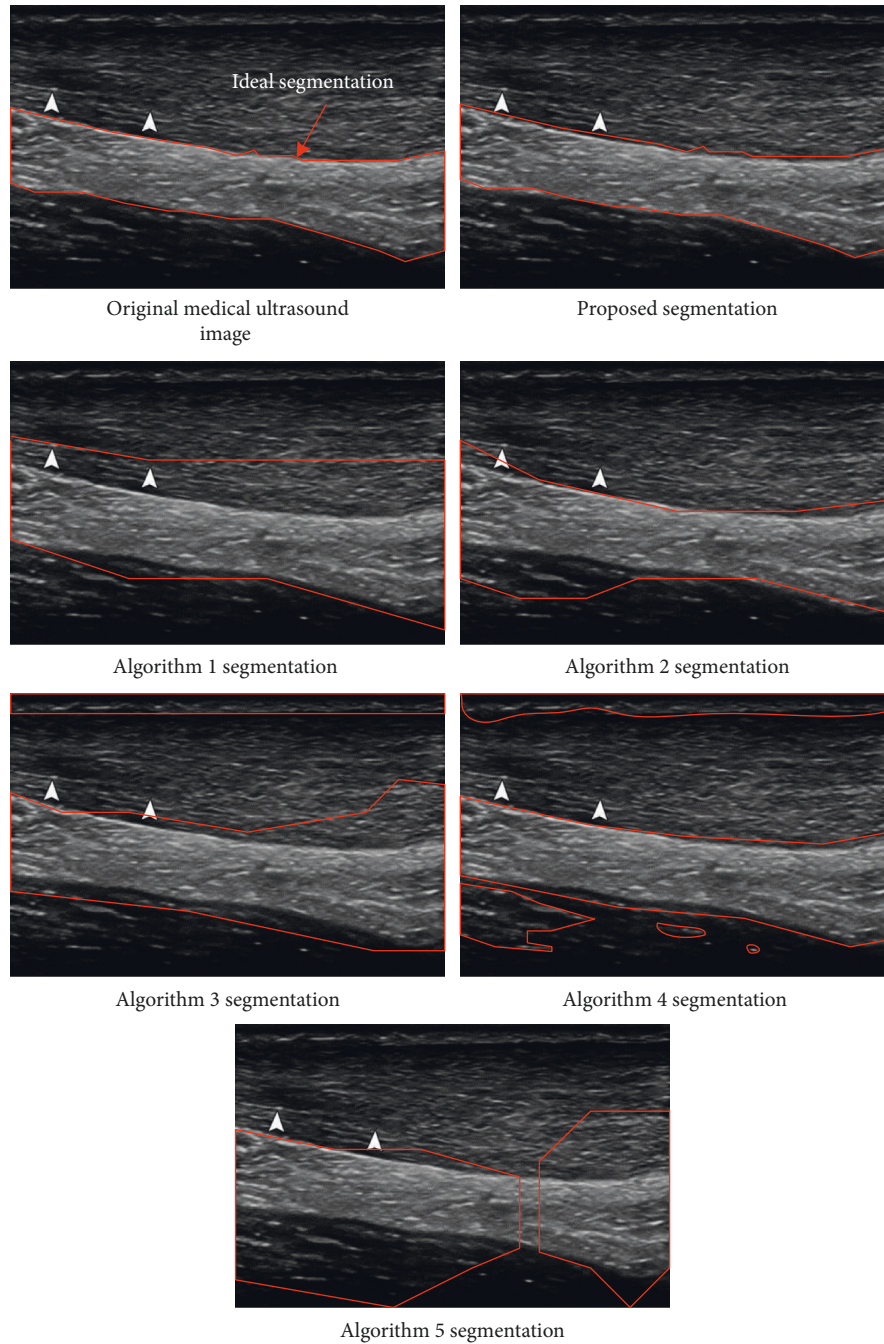


FIGURE 5: Comparison of segmentation effect test results of different segmentation algorithms.

algorithms. It can be proved that the segmentation error of the proposed segmentation algorithm is small, and the segmentation algorithm is effective.

Randomly select an image in the MedPix data set for the segmentation effect test. Based on the above test results, the segmentation effects of the above six image segmentation algorithms are tested, and the test results are shown in Figure 5.

According to the analysis of Figure 5, the image segmentation effect of the proposed algorithm is consistent with the ideal target segmentation effect, while the segmentation effects detected by other segmentation algorithms are lower than the test results of the proposed algorithm, in which

algorithms 1–3 are inconsistent with the ideal segmentation effect, while algorithms 4 and 5 also have excessive segmentation. It can be proved that the proposed algorithm has an excellent segmentation effect in image segmentation, which proves that the segmentation algorithm has high effectiveness and superior segmentation performance.

4. Conclusions

With the continuous progress of image processing technology, the image segmentation algorithm has become one of the important technologies to assist doctors in diagnosis.

Aiming at the problems existing in the traditional image segmentation algorithm, a human motion injury ultrasonic medical image segmentation algorithm based on deep feature fusion is proposed. The algorithm trains SVM according to the image feature fusion results and completes the segmentation of human motion injury image through the eigenvalue output of SVM. The experimental results show that the average accuracy of the athlete's posture of the algorithm is 95.97%. The segmentation time of ultrasonic medical images of human motion injury in this paper is less than 150 ms. The convergence of the algorithm is completed when the number of iterations is 3. The maximum segmentation error rate is 2.68%. The image segmentation effect is consistent with the ideal target segmentation effect. However, there are some problems in the design process of the algorithm. The algorithm has some errors in enhancing the effect of image segmentation. In view of this problem, we will continue to optimize the segmentation algorithm until the algorithm is perfect, so as to further improve the quality of the ultrasonic medical image segmentation algorithm for human motion injury.

Data Availability

The data that support the findings of this study are available from the corresponding author upon reasonable request.

Conflicts of Interest

The authors declare that there are no conflicts of interest with any financial organizations regarding the material reported in this manuscript.

References

- [1] H. S. Munawar, A. W. Hammad, and S. T. Waller, "A review on flood management technologies related to image processing and machine learning," *Automation in Construction*, vol. 132, no. 8, Article ID 103916, 2021.
- [2] Q. Yun and C. Leng, "Intelligent control of urban lighting system based on video image processing technology," *IEEE Access*, vol. 8, Article ID 155506, 2020.
- [3] S. Yan, X. C. Tai, J. Liu, and H. Y. Huang, "Convexity shape prior for level set-based image segmentation method," *IEEE Transactions on Image Processing*, vol. 29, pp. 7141–7152, 2020.
- [4] X. Liu, Y. Zhang, H. Jing, L. Wang, and S. Zhao, "Ore image segmentation method using U-Net and Res_Unet convolutional networks," *RSC Advances*, vol. 10, no. 16, pp. 9396–9406, 2020.
- [5] K. M. Sediqi and H. J. Lee, "A novel upsampling and context convolution for image semantic segmentation," *Sensors*, vol. 21, no. 6, p. 2170, 2021.
- [6] W. Lin and Y. Li, "Parallel regional segmentation method of high-resolution remote sensing image based on minimum spanning tree," *Remote Sensing*, vol. 12, no. 5, p. 783, 2020.
- [7] J. Xue, Y. Wang, and A. Qu, "Image segmentation method for Lingwu long jujubes based on improved FCN-8s," *Transactions of the Chinese Society of Agricultural Engineering*, vol. 37, no. 5, pp. 191–197, 2021.
- [8] R. Sami, S. Soltane, and M. Helal, "Microscopic image segmentation and morphological characterization of novel chitosan/silica nanoparticle/nisin films using antimicrobial technique for blueberry preservation," *Membranes*, vol. 11, no. 5, 303 pages, 2021.
- [9] R. Schmitz, F. Madesta, M. Nielsen et al., "Multi-scale fully convolutional neural networks for histopathology image segmentation: from nuclear aberrations to the global tissue architecture," *Medical Image Analysis*, vol. 70, no. 12, Article ID 101996, 2021.
- [10] W. Li, Z. Luo, and X. Xi, "Movement trajectory recognition of sign language based on optimized dynamic time warping," *Electronics*, vol. 9, no. 9, pp. 1400–1412, 2020.
- [11] H. Xue, D. Q. Huynh, and M. Reynolds, "A location-velocity-temporal attention LSTM model for pedestrian trajectory prediction," *IEEE Access*, vol. 8, Article ID 44576, 2020.
- [12] G. Shuqing and S. Yucong, "Traffic sign recognition based on HOG feature extraction," *Journal of Measurements in Engineering*, vol. 9, no. 3, pp. 142–155, 2021.
- [13] A. Dmd, B. Sjr, and C. Ds, "Multi objective optimization of fused deposition modeling process parameters with desirability function - ScienceDirect," *Procedia CIRP*, vol. 99, pp. 707–710, 2021.
- [14] H. Yang, B. Zhou, Q. Wei, X. Wang, X. Xu, and R. Zhang, "Accurate attitude estimation of HB2 standard model based on QNCF in hypersonic wind tunnel test," *Chinese Journal of Aeronautics*, vol. 33, no. 1, pp. 64–72, 2020.
- [15] F. Muñoz-Muñoz and A. Rodrigo-Mor, "Partial discharges and noise discrimination using magnetic antennas, the cross wavelet transform and support vector machines," *Sensors*, vol. 20, no. 11, 3180 pages, 2020.
- [16] M. C. Klein and E. Roberts, "Automatic error control during forward flux sampling of rare events in master equation models," *The Journal of Chemical Physics*, vol. 152, no. 3, Article ID 035102, 2020.
- [17] H. Rastgoftar, E. M. Atkins, and I. V. Kolmanovskiy, "Scalable vehicle team continuum deformation coordination with eigen decomposition," *IEEE Transactions on Automatic Control*, vol. 67, no. 5, pp. 2514–2521, 2022.
- [18] Y. Alammari, I. Iovkov, S. Berger, J. Saelzer, and D. Biermann, "Adhesion area estimation using backscatter image gray level masking of uncoated tungsten carbide tools," *Wear*, vol. 476, no. 1, Article ID 203666, 2021.
- [19] D. Zerbst, C. Liebold, T. Gereke, A. Haufe, S. ClauB, and C. Cherif, "Modelling inhomogeneity of veneer laminates with a finite element mapping method based on arbitrary grayscale images," *Materials*, vol. 13, no. 13, p. 2993, 2020.
- [20] J. Xi, J. Chen, Z. Wang et al., "Simultaneous segmentation of fetal hearts and lungs for medical ultrasound images via an efficient multi-scale model integrated with attention mechanism," *Ultrasonic Imaging*, vol. 43, no. 6, pp. 308–319, 2021.